51st AIAA Aerospace Sciences Meeting including the New Horizons Forum and Aerospace Exposition
07 - 10 January 2013, Grapevine (Dallas/Ft. Worth Region), Texas

AIAA 2013-0303

Comparison of Models for Mixture Transport Properties for Numerical Simulations of Ablative Heat-Shields

Hicham Alkandry[*] and Iain D. Boyd[†]

Department of Aerospace Engineering, University of Michigan, Ann Arbor, MI

Alexandre Martin[‡]

Department of Mechanical Engineering, University of Kentucky, Lexington, KY

The goal of this study is to evaluate the effects of different models for calculating the mixture transport properties on flowfield predictions of ablative heat-shields. The Stardust sample return capsule at four different trajectory conditions is used as a test case for this study. In the first part of the study, the results predicted using Wilke's mixing rule with species viscosities calculated using Blottner's curve fits and species thermal conductivities determined using Eucken's relation are compared to the results obtained using Gupta's mixing rule with collision cross-section (CCS) data. The Wilke/Blottner/Eucken model overpredicts the heat transfer to the surface relative to the Gupta/CCS model by as much as 60%. The Wilke/Blottner/Eucken model also overpredicts the mass blowing rate due to the removal of bulk carbon by as much as 25% compared to the Gupta/CCS model. In the second part of the study, the effects of the mass diffusion model are assessed using Fick's, modified Fick's, self-consistent effective binary diffusion (SCEBD), and Stefan-Maxwell models. The results show that the flowfield properties calculated using modified Fick's, SCEBD, and Stefan-Maxwell models are in good agreement. Fick's model overpredicts the heat transfer and mass blowing rate by as much as 20% relative to the Stefan-Maxwell model.

Nomenclature

D_s	Diffusion coefficient of species s, m^2/s
$D_{s,r}$	Binary diffusion coefficient of species s and r, m^2/s
J_s	Mass diffusion flux of species s, kg/m^2/s
k_B	Boltzmann constant, 1.38×10^{-23} kg·m^2/s^2/K
M	Average molar weight of the gas-phase mixture, kg/mol
M_s	Molar weight of species s, kg/mol
N_{av}	Avogadro's number, 6.022×10^{23} mol^{-1}
NS	Number of gas-phase species
p	Pressure, Pa
p_s	Partial pressure of species s, Pa
R	Universal gas constant, 8.314 J/mol/K
T_{tr}	Translational/rotational temperature, K
T_{ve}	Vibrational/electronic/electron temperature, K
X_s	Mole fraction of species s
Y_s	Mass fraction of species s
κ	Coefficient of thermal conductivity, W/m/K
μ	Coefficient of viscosity, Pa·s

[*]Research Fellow, Member AIAA.
[†]James E. Knott Professor of Engineering, Fellow AIAA.
[‡]Assistant Professor, Senior Member AIAA.

American Institute of Aeronautics and Astronautics

ρ Density, kg/m^3

ρ_s Partial density of species s, kg/m^3

I. Introduction

Many planetary entry vehicles employ an ablative thermal protection system (TPS) in order to sustain the very large heat fluxes experienced during atmospheric entry. The hypersonic flow around these entry vehicles interacts with the TPS, which may cause some ablation by-products to be transported across the boundary layer into the flowfield. Several models exist to simulate these transport phenomena using computational fluid dynamics (CFD). These models, however, may give different transport properties, which can have a significant effect on the predicted flowfield and heat transfer to the entry vehicle. Therefore, the goal of this study is to assess the effects of transport models on CFD predictions of ablative heat-shields. Several other studies have investigated the effects of the mixture transport models on the predicted flowfield and surface properties of planetary entry vehicles.[1–5] These studies have shown that the mixture transport model can have an important effect on the predicted flowfield and heat transfer to the entry vehicles. However, these studies have mainly focused on catalytic non-ablative TPS materials. The current study aims to extend the analysis to CFD simulations of ablative heat-shields and consider models for both the mixture transport coefficients (i.e. viscosity, thermal conductivity, and mass diffusion) and mass diffusion fluxes.

For this study, CFD simulations are performed using the re-entry conditions for the Stardust sample return capsule. In the first part of the study, the effects of two different models for calculating the mixture transport coefficients are investigated. The first model considered in this study is Wilke's semi-empirical mixing rule with species viscosities and thermal conductivities determined using Blottner's curve fits and Eucken's relation, respectively. The second model is Gupta's mixing rule using collision cross-section data to determine the viscosity and thermal conductivity of individual species. The effects of the mass diffusion model are assessed in the second part of the study using Fick's model, modified Fick's model, the self-consistent effective binary diffusion (SCEBD) model, and the Stefan-Maxwell model. The paper is presented as follows. First, the CFD code and formulation of the different models used in this study are described. Then, details about the Stardust sample return capsule and numerical setup are provided. Finally, the numerical results obtained using these models for the transport phenomena are presented and discussed.

II. Governing Equations

The numerical simulations are performed using the CFD code LeMANS, which is developed at the University of Michigan.[6,7] LeMANS solves the laminar Navier-Stokes equations on unstructured computational grids including thermo-chemical nonequilibrium effects with second-order spatial accuracy. In LeMANS, the flow is modeled assuming that the continuum approximation is valid. Furthermore, for this study, it is assumed that the translational and rotational energy modes can be described by a single temperature T_{tr}, and that the vibrational, electronic, and electron translational energy modes are described by a different temperature T_{ve}. The finite-volume method is used to solve the set of partial differential equations. A modified Steger-Warming Flux Vector Splitting scheme[8] is used to discretize the inviscid fluxes across cell faces, which is less dissipative and produces better results in boundary layers compared to the original scheme. The viscous terms are computed using cell-centered and nodal values. The viscous stresses are modeled assuming a Newtonian fluid and Stokes' hypothesis, and the heat fluxes are modeled according to Fourier's law for all temperatures. A finite-rate surface chemistry module originally developed by Marschall and MacLean[9,10] has been implemented in LeMANS to model the interaction between the hypersonic gas flow and the vehicle surface.[11] This module allows for the specification of several different surface reaction processes, including adsorption/desorption, Eley-Rideal recombination, and oxidation/nitridation. The module calculates the species production rates at the surface based on the pressure, temperature, and species concentrations at the wall. The effects of pyrolysis gases emitted from the surface are neglected in this study and the only contribution to the mass blowing rate is due to the removal of bulk species by surface reactions such as oxidation. LeMANS is parallelized using METIS[12] to partition the computational mesh, and the Message Passing Interface (MPI) to communicate the necessary information between processors.

American Institute of Aeronautics and Astronautics

A. Mixture Transport Coefficients

1. Wilke/Blottner/Eucken

The Wilke/Blottner/Eucken model is the first model considered in this study for calculating the mixture transport coefficients. This model employs Wilke's mixing rule,[13] which is a simplification of the full first-order Chapman-Enskog relation, along with curve fits determined by Blottner et al.[14] for the species viscosities and Eucken's relation[15] for the species thermal conductivities. Wilke's mixing rule has been shown to produce adequate results for relatively slow speeds for which the maximum temperature in the flowfield is around 10,000 K.[4,5] Using this model, the mixture viscosity and thermal conductivity for each energy mode can be calculated as an appropriately weighted sum of the individual species viscosities and thermal conductivities by,

$$\mu = \sum_s \frac{X_s \mu_s}{\phi_s} \qquad \text{and} \qquad \kappa = \sum_s \frac{X_s \kappa_s}{\phi_s} \tag{1}$$

where the scaling factor ϕ_s is given by

$$\phi_s = \sum_r X_r \left[1 + \sqrt{\frac{\mu_s}{\mu_r}} \left(\frac{M_r}{M_s} \right)^{1/4} \right]^2 \left[\sqrt{8 \left(1 + \frac{M_s}{M_r} \right)} \right]^{-1} \tag{2}$$

The coefficient of viscosity of each species is calculated using Blottner's curve fits[14] as

$$\mu_s = 0.1 \exp \left[(A_s \ln T_{tr} + B_s) \ln T_{tr} + C_s \right] \tag{3}$$

where A, B, and C are constants determined for each species.

The coefficient of thermal conductivity for the translational/rotational and vibrational/electronic/electron energy modes can be calculated using Eucken's relation,[15]

$$\kappa_{tr,s} = \frac{5}{2} \mu_s C_{v_{t,s}} + \mu_s C_{v_{r,s}} \qquad\qquad \kappa_{ve,s} = \mu_s C_{v_{ve,s}} \tag{4}$$

where $C_{v_{t,r,ve}}$ are the specific heats at constant volume for each internal energy mode.

The effective, or average, diffusion coefficient for each species is replaced by a single coefficient calculated using the mixture coefficient of thermal conductivity and given by,

$$D_s = D = \frac{\kappa_{tr} Le}{\rho C_{p_{tr}}} \tag{5}$$

where $C_{p_{tr}}$ is the mixture translational/rotational specific heat at constant pressure, and Le is the Lewis number which is assumed to be constant. For this study, the Lewis number is assumed to be equal to 1.4.

2. Gupta/Collision Cross-Section Data

Gupta et al.[16] developed another model for calculating the mixture transport properties for weakly ionized flows. This model is considered to be more physically accurate than the Wilke/Blottner/Eucken model because it takes into account the collision integrals in the multi-component mixture.[4] These collision integrals are evaluated at a controlling temperature for each collision pair. For collisions between two heavy particles, the controlling temperature is chosen as the translational/rotational temperature T_{tr}. The vibrational/electron/electronic temperature, T_{ve}, is used as the controlling temperature for collisions involving electrons. Gupta's mixing rule has also been shown to be more numerically efficient than Wilke's mixing rule because it requires fewer calls to the power (exponent) and square root functions.[4] Using Gupta's mixing rule, the mixture viscosity can be calculated by,

$$\mu = \sum_{s \neq e} \frac{m_s \gamma_s}{\sum\limits_{r \neq e} \gamma_r \Delta_{s,r}^{(2)}(T_{tr}) + \gamma_e \Delta_{s,e}^{(2)}(T_{ve})} + \frac{m_e \gamma_e}{\sum\limits_r \gamma_r \Delta_{e,r}^{(2)}(T_{ve})} \tag{6}$$

where the collision terms $\Delta_{s,r}$ are evaluated at the different controlling temperatures T_{tr} and T_{ve}. The molar concentration of each species, γ_s, can be calculated by,

$$\gamma_s = \frac{\rho_s}{\rho M_s} \tag{7}$$

American Institute of Aeronautics and Astronautics

The mass of each species, m_s, is given by,

$$m_s = \frac{M_s}{N_{av}} \tag{8}$$

The mixture thermal conductivity for the translational mode can be calculated by,

$$\kappa_t = \frac{15}{4} k_B \sum_{s \neq e} \frac{\gamma_s}{\sum\limits_{r \neq e} a_{s,r} \gamma_r \Delta_{s,r}^{(2)}(T_{tr}) + 3.54 \gamma_e \Delta_{s,e}^{(2)}(T_{ve})} \tag{9}$$

where,

$$a_{s,r} = 1 + \frac{[1 - (m_s/m_r)] [0.45 - 2.54(m_s/m_r)]}{[1 + (m_s/m_r)]^2} \tag{10}$$

The thermal conductivity for the rotational mode is given by,

$$\kappa_r = k_B \sum_{s=mol} \frac{\gamma_s}{\sum\limits_{r \neq e} \gamma_r \Delta_{s,r}^{(1)}(T_{tr}) + \gamma_e \Delta_{s,e}^{(1)}(T_{ve})} \tag{11}$$

where the summation s is over all the molecules. The mixture thermal conductivity for the translational/rotational mode is equal to the sum of the conductivity for the translational (Equation 9) and the rotational (Equation 11) modes,

$$\kappa_{tr} = \kappa_t + \kappa_r \tag{12}$$

The thermal conductivity for the vibrational/electronic mode can be calculated by,

$$\kappa_{vel} = k_B \frac{C_{v_{ve}}}{R} \sum_{s=mol} \frac{\gamma_s}{\sum\limits_{r \neq e} \gamma_r \Delta_{s,r}^{(1)}(T_{tr}) + \gamma_e \Delta_{s,e}^{(1)}(T_{ve})} \tag{13}$$

The thermal conductivity for electrons is given by,

$$\kappa_e = \frac{15}{4} k_B \frac{\gamma_e}{\sum\limits_{r} 1.45 \gamma_r \Delta_{e,r}^{(2)}(T_{ve})} \tag{14}$$

The collision terms, $\Delta_{s,r}^{(1)}$ and $\Delta_{s,r}^{(2)}$, can be calculated by,

$$\Delta_{s,r}^{(1)} = \frac{8}{3} \left[\frac{2M_s M_r}{\pi R T (M_s + M_r)} \right]^{1/2} \pi \bar{\Omega}_{s,r}^{(1,1)} \tag{15}$$

$$\Delta_{s,r}^{(2)} = \frac{16}{5} \left[\frac{2M_s M_r}{\pi R T (M_s + M_r)} \right]^{1/2} \pi \bar{\Omega}_{s,r}^{(2,2)} \tag{16}$$

where the collision integrals $\pi \bar{\Omega}_{s,r}^{(1,1)}$ and $\pi \bar{\Omega}_{s,r}^{(2,2)}$ can be determined using several different methods that usually rely on modeling the interaction potential for a pair of particles and integrating the differential cross-section obtained from that potential over the entire solid angle space.[16–18]

The binary diffusion coefficient involving two heavy particles is given by,

$$D_{s,r} = \frac{k_B T_{tr}}{p \Delta_{s,r}^{(1)}(T_{tr})} \tag{17}$$

and for electrons as,

$$D_{e,r} = \frac{k_B T_{ve}}{p \Delta_{e,r}^{(1)}(T_{ve})} \tag{18}$$

An effective diffusion coefficient can be defined by regarding the multi-component mixture as a binary mixture made up of species s and a composite species that represents all of the other species. This effective diffusion coefficient for species s is calculated by,

$$D_s = (1 - X_s) \left(\sum_{r \neq s, e} \frac{X_r}{D_{s,r}} \right)^{-1} \tag{19}$$

American Institute of Aeronautics and Astronautics

B. Mass Diffusion

1. Fick's Model

In a binary system with two chemical species s and r, Fick's law of diffusion states that each species moves relative to the mixture in the direction of decreasing mole fraction.[19] In terms of mass diffusion flux, Fick's law can be written as,

$$J_s = -\rho D_{s,r} \nabla Y_s \tag{20}$$

Fick's law can be extended to a mixture of three or more species by replacing the binary diffusion coefficient $D_{s,r}$ by the effective diffusion coefficient D_s. The mass diffusion fluxes for heavy species is calculated as,

$$J_{s \neq e} = -\rho D_s \nabla Y_s \tag{21}$$

The electron mass diffusion flux is calculated assuming ambipolar diffusion to ensure charge neutrality of the flow. It is given by,

$$J_e = -\frac{1}{q_e} \sum_{s \neq e} q_s J_s \tag{22}$$

where q_s is the charge per unit mass of species s.

2. Modified Fick's Model

Fick's model as defined in Equation 21 does not enforce the requirement that the diffusion mass fluxes sum to zero.[1] Therefore, a modified version of Fick's model is also considered in this study which ensures that the sum of the diffusion mass fluxes is zero. The mass diffusion flux for heavy species using the modified Fick's model can be calculated by,

$$J_{s \neq e} = -\rho D_s \nabla Y_s - Y_s \sum_{r \neq e} -\rho D_r \nabla Y_r \tag{23}$$

The electron diffusion flux is calculated using Equation 22 assuming ambipolar diffusion to enforce charge neutrality.

3. Self-Consistent Effective Binary Diffusion (SCEBD) Model

Another model considered in this study is the self-consistent effective binary diffusion method, which was originally developed for computational simulations of multi-component plasma flows.[20,21] The SCEBD model makes use of the small electron mass approximation to simplify the mass diffusion flux equations and the calculation of the electronic field in weakly ionized flows. The heavy species mass diffusion fluxes are determined by,

$$J_{s \neq e} = -\frac{p M_s D_s}{R T_{tr}} \nabla \left(\frac{p_s}{p} \right) + Y_s \sum_{r \neq e} \frac{p M_r D_r}{R T_{tr}} \nabla \left(\frac{p_r}{p} \right) + \frac{1}{R T_{tr}} \left[M_s q_s \rho_s D_s - Y_s \sum_{r \neq e} M_r q_r \rho_r D_r \right] E \tag{24}$$

where the electric field E is defined as,

$$E = \frac{p}{q_e \rho_e} \nabla \left(\frac{p_e}{p} \right) \tag{25}$$

The electron diffusion flux, J_e, can then be calculated using Equation 22.

In the SCEBD model, the expression for the effective diffusion coefficient given in Equation 19 is replaced by,

$$D_{s \neq e} = \left(1 - \frac{\omega_s}{\omega} \right) \left(\sum_{r \neq s,e} \frac{p_r}{p D_{sr}} \right)^{-1} \tag{26}$$

where ω_s/ω are weighting factors defined as,

$$\frac{\omega_s}{\omega} = \frac{\rho_s / \sqrt{M_s}}{\sum_{r \neq e} \left(\rho_r / \sqrt{M_r} \right)} \tag{27}$$

Note that this choice of weighting factor represents a geometric mean of the conventional choice $\omega_s/\omega = X_s$ and the intuitive choice $\omega_s/\omega = Y_s$.[20]

American Institute of Aeronautics and Astronautics

4. Stefan-Maxwell Model

The Stefan-Maxwell equation was originally developed to solve for the mole fraction gradient as,

$$\nabla X_s = \frac{M}{\rho} \sum_{r \neq s} \left(\frac{X_s J_r}{M_r D_{s,r}} - \frac{X_r J_s}{M_s D_{s,r}} \right) \tag{28}$$

This equation can be re-arranged to solve for the mass diffusion fluxes in terms of the mass fraction gradient,[1]

$$J_s = -\rho D_s \nabla Y_s + \frac{Y_s}{(1 - X_s)} D_s \sum_{r \neq s} \left(\rho \frac{M}{M_r} \nabla Y_r + \frac{M}{M_r} \frac{J_r}{D_{s,r}} \right) \tag{29}$$

Equation 29 is a set of (NS−1) equations for NS species, and therefore a closure relation is needed to find the mass diffusion fluxes. For this study, an iterative method is used to solve for the fluxes.[1] First, the mass flux for each heavy species is calculated at iteration N using,[1,2]

$$J_{s \neq e}^N = -\rho D_s \nabla Y_s + \frac{Y_s}{(1 - X_s)} D_s \sum_{r \neq s,e} \left(\rho \frac{M}{M_r} \nabla Y_r + \frac{M}{M_r} \frac{J_r^{N-1}}{D_{s,r}} \right) \tag{30}$$

then the entire set is corrected for iteration N+1 using the closure equation,

$$J_{s \neq e}^{N+1} = J_s^N - Y_s \sum_{r \neq e} J_r^N \tag{31}$$

The first term of Equation 30 is used as the initial guess in the iteration process. The electron mass diffusion flux is then determined using Equation 22. The Stefan-Maxwell model has been shown to accurately calculate the mass diffusion fluxes for multi-component mixtures[1,5] and is considered the most physically rigorous model in this study. One drawback of the Stefan-Maxwell model, however, is that it is computationally expensive and has been shown to require approximately 50% more time per iteration than the other models.[1]

III.   Test Case - Stardust Sample Return Capsule

The Stardust payload was launched in 1999 on a mission to collect samples from interstellar dust and the tail of the Comet Wild-2, and return them to Earth. The Stardust sample return capsule (SRC), shown schematically in Figure 1(a), landed in the Utah desert in January of 2006. The Earth entry trajectory of the return capsule is presented in Figure 1(b). The Stardust spacecraft then continued its travel through the solar system, on a mission to image Comet Tempel-1. It was decommissioned after completing that final mission in March 2011. The Stardust mission represents the first ever return of a sample from a comet; a significant milestone in the human exploration of space. With an entry velocity of 12.6 km/s, the capsule was also the fastest man-made object ever to enter the Earth's atmosphere, providing a unique test case to evaluate numerical simulations. In order to protect the vehicle from the extreme entry conditions, the thermal protection system for the Stardust capsule used the phenolic-impregnated carbon ablator (PICA),[22] which is a lightweight material with a density of approximately 240 kg/m^3.

The freestream conditions simulated in this study are listed in Table 1.[23] Peak heating occurs at an altitude of 62 km approximately 51 sec after atmospheric entry. The chemistry model for the gas environment is adapted from Ref. 24, and consists of the following nineteen species:

$$N_2, O_2, NO, N, O, N_2^+, O_2^+, NO^+, N^+, O^+, e$$

$$C, C_2, C_3, CO, CO_2, CN, CO^+, C^+$$
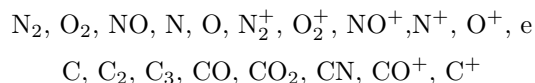
The constants used in Blottner's curve fits (i.e. Equation 3) for the gas-phase species considered in this study are presented in Table 2. These constants are determined using the commercial software CHEMKIN to produce temperature-dependent viscosity curve fits for each individual species.[25] The collision integrals used in this study are based on the data collected by Wright et al. in Refs. 17, 18. The collision integrals involving ions and neutrals are based on the polarization potential, which is a function only of dipole polarizability of the neutral species and the temperature. For interactions between two charged particles
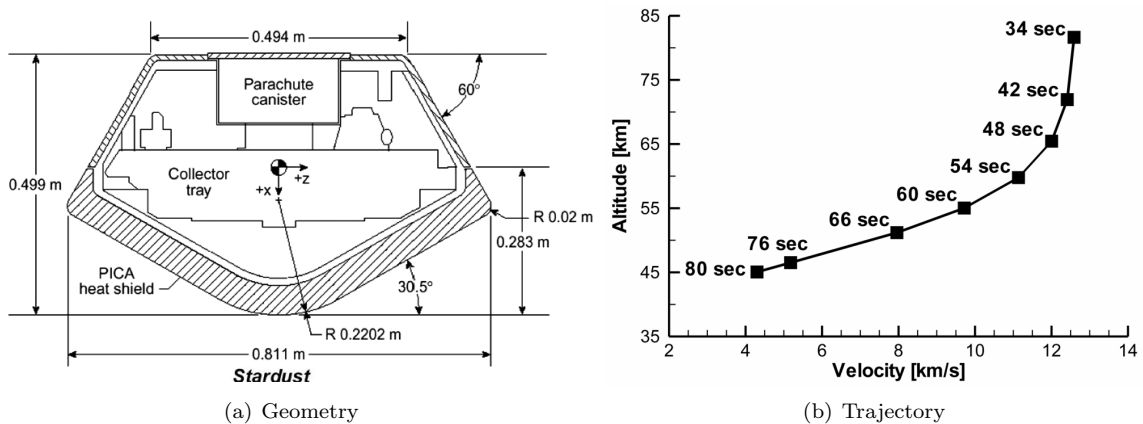
American Institute of Aeronautics and Astronautics

(a) Geometry

(b) Trajectory

Figure 1. Stardust sample return capsule geometry and entry trajectory.

Table 1. Freestream conditions.

Time from entry, sec	Altitude, km	Velocity, m/sec	Density, kg/m^3	Temperature, K
42	71	12,060	5.6×10^{-5}	222
51	62	10,870	2.1×10^{-4}	235
61	54	8,070	5.9×10^{-4}	251
66	51	6,500	8.5×10^{-4}	256

Table 2. Blottner curve fit coefficients.

Species	A	B	C
N_2	2.68E-02	3.18E-01	-1.13E+01
O_2	4.49E-02	-8.26E-02	-9.20E+00
NO	4.36E-02	-3.36E-02	-9.58E+00
N	1.16E-02	6.03E-01	-1.24E+01
O	2.03E-02	4.29E-01	-1.16E+01
N_2^+	2.68E-02	3.18E-01	-1.13E+01
O_2^+	4.49E-02	-8.26E-02	-9.20E+00
NO^+	3.02E-01	-3.50E+00	-3.74E+00
N^+	1.16E-02	6.03E-01	-1.24E+01
O^+	2.03E-02	4.29E-01	-1.16E+01
C	-1.00E-04	7.93E-01	-1.34E+01
C_2	-3.10E-03	6.92E-01	-1.26E+01
C_3	-1.47E-02	8.81E-01	-1.35E+01
CO	-1.95E-02	1.01E+00	-1.40E+01
CO_2	-1.95E-02	1.05E+00	-1.43E+01
CN	2.50E-03	6.81E-01	-1.25E+01
CO^+	-1.95E-02	1.01E+00	-1.40E+01
C^+	-8.33E-03	7.70E-01	-1.27E+01
e	0	0	-1.20E+01

American Institute of Aeronautics and Astronautics

(electron-electron, electron-ion, and ion-ion), the collision integrals are calculated using attractive and repulsive shielded coulomb potentials.

Table 3 presents the chemical mechanisms that are assumed to occur at the surface of the Stardust SRC. These mechanisms were developed by Driver et al. by comparing CFD predictions to heat transfer and recession rate measurements obtained at an arc-jet facility for PICA.[26, 27] The mechanisms found by Driver et al. include the oxidation of bulk carbon by atomic oxygen with a constant reaction efficiency of $\gamma = 0.90$, and the oxidation of bulk carbon by molecular oxygen with a constant efficiency of $\gamma = 0.01$. These mechanisms also include the recombination of atomic nitrogen at the surface with a constant recombination efficiency of $\gamma = 0.05$. Table 3 also presents the heat released by these exothermic surface reactions.

Table 3. Surface chemical reactions.[26, 27]

#	Reaction	Efficiency
1	$O + C(b) \rightarrow CO$, $\Delta H = 360$ kJ/mol	0.90
2	$O_2 + 2C(b) \rightarrow 2CO$, $\Delta H = 217$ kJ/mol	0.01
3	$N + N \rightarrow N_2$, $\Delta H = 950$ kJ/mol	0.05

The surface material of the Stardust entry capsule for this study is assumed to be FiberForm, instead of PICA. FiberForm is the substrate from which PICA is processed, and has been shown to have approximately the same properties as the char layer of PICA.[28] This assumption is chosen to neglect the effects of pyrolysis gases emitted from the surface since FiberForm does not contain phenolic. The density of the bulk environment is assumed to be equal to 180 kg/m^3, which is the density of FiberForm and PICA close to the char exterior surface.[28] The surface temperature is calculated assuming radiative equilibrium at the wall with an emissivity of 0.9. The entry of the Stardust SRC was nearly ballistic.[29] Therefore, a two-dimensional axisymmetric grid is used in this study. The grid is composed of approximately 96,000 quadrilateral cells in the forebody region, with approximately 300 cells in the axial direction and 320 cells in the radial direction along the SRC forebody. Clustering is used near the capsule surface and the size of the first grid cell from the wall is 10^{-6} m.

IV. Results

The goal of this study is to evaluate the effects of different models for transport phenomena used in CFD codes on the flowfield predictions of ablative heat-shields. The numerical results are presented in two sections. The first section discusses the effects of the model for the mixture transport coefficients (viscosity, thermal conductivity, and mass diffusion) on the flowfield solutions of the Stardust SRC using the Wilke/Blottner/Eucken and Gupta/CCS models. The species mass diffusion fluxes for both sets of cases are calculated using the modified Fick's model. The second part describes the effects of the mass diffusion model on the Stardust SRC solutions using Fick's, modified Fick's, SCEBD, and Stefan-Maxwell models. The transport coefficients are calculated using the Gupta/CCS model in this second portion of the study.

A. Mixture Transport Coefficients

Figure 2 presents the stagnation point heat transfer to the Stardust SRC as a function of freestream velocity calculated using the Wilke/Blottner/Eucken and Gupta/CCS models. Figure 2(a) shows the solution obtained using the surface chemistry mechanisms given in Table 3, while Figure 2(b) shows the non-catalytic wall solution with no surface reactions. For the finite-rate surface chemistry solution, the heat transfer obtained using the Wilke/Blottner/Eucken model is in good agreement with the Gupta/CCS solution for the 51 km conditions. However, the Wilke/Blottner/Eucken model overpredicts the heat transfer relative to the Gupta/CCS model by about 15% for 54 km, 35% for 62 km, and 60% for 71 km. The non-catalytic wall solution also follows a similar trend as can be seen in Figure 2(b). However, the difference in the heat transfer predicted using the Wilke/Blottner/Eucken and Gupta/CCS models is smaller for the non-catalytic wall. This result shows that the transport coefficients model can have a significant effect on the predicted heat transfer for ablative heat-shields.

The heat transfer to the Stardust SRC surface includes the contribution due to temperature gradients (convective) and the diffusion of enthalpy (diffusive). Figure 3 presents the convective and diffusive
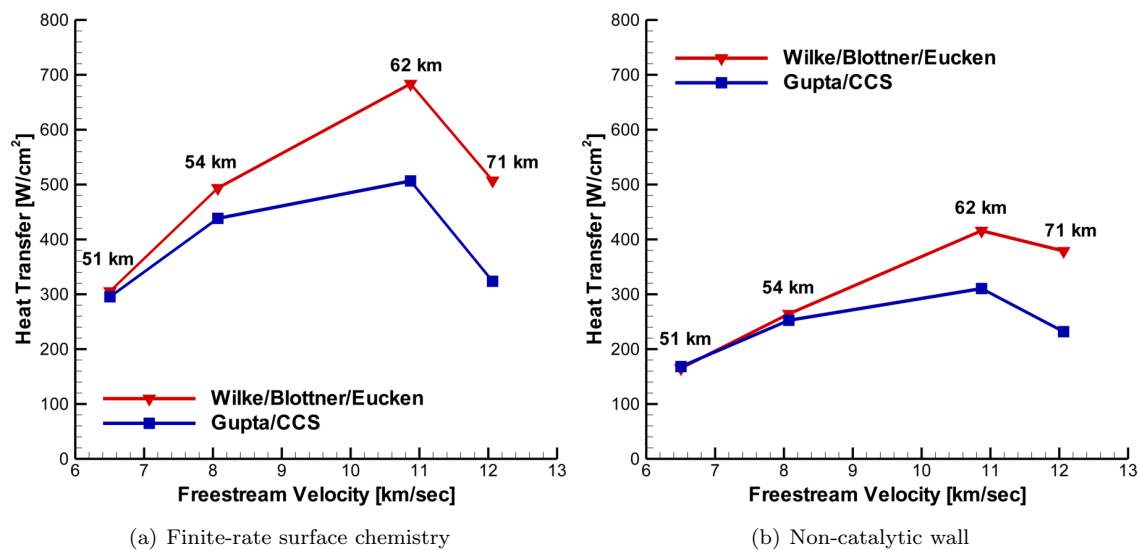
Figure 2. Stagnation point heat transfer calculated using the Wilke/Blottner/Eucken and Gupta/CCS models.

heat transfer components at the stagnation point as functions of freestream velocity calculated using the Wilke/Blottner/Eucken and Gupta/CCS models. Figure 3(a) shows that the transport models produce similar convective heat transfer for the 51 km and 54 km conditions. However, the Wilke/Blottner/Eucken model produces a greater convective heat transfer compared to the Gupta/CCS model for the 62 km and 71 km trajectory points by about 20% and 60%, respectively. The Wilke/Blottner/Eucken model also produces a larger diffusive heat transfer relative to the Gupta/CCS model as can be seen in Figure 3(b). The difference in the predicted diffusive heat transfer varies from about 10% for the 51 km conditions to 60% for the 71 km conditions. This difference in the diffusive component between the Wilke/Blottner/Eucken and Gupta/CCS models increases the disagreement in the heat transfer between the two models compared to the non-catalytic wall solution as can be seen in Figure 2.
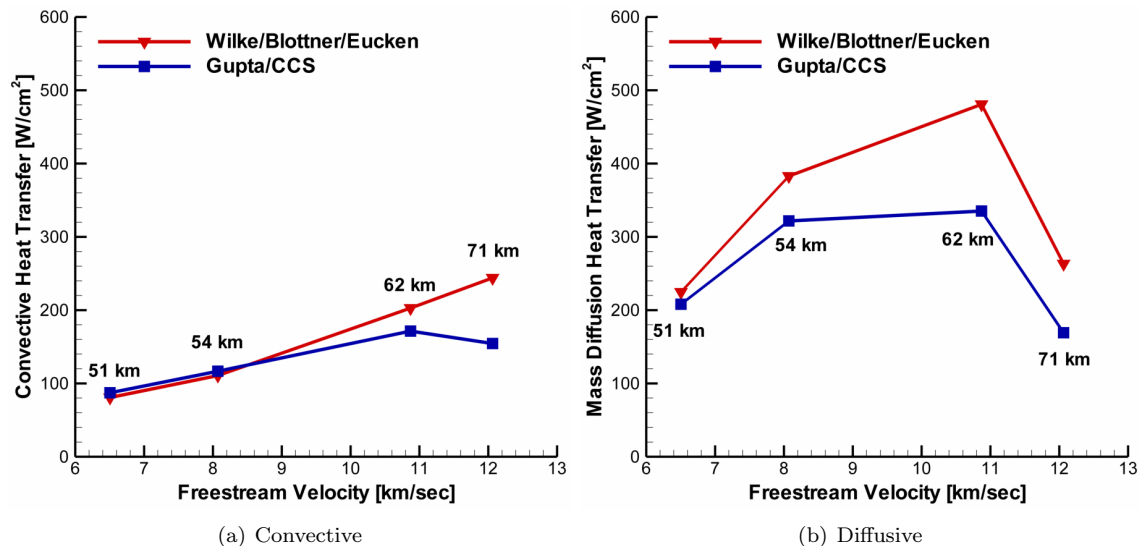

Figure 3. Convective and diffusive stagnation point heat transfer calculated using the Wilke/Blottner/Eucken and Gupta/CCS models.

The removal of bulk carbon due to the oxidation reactions (Table 3) produces an effective mass blowing at the surface. The rate of this mass blowing at the stagnation point calculated using the Wilke/Blottner/Eucken and Gupta/CCS models is presented in Figure 4. The blowing rate calculated using the Wilke/Blottner/Eucken

American Institute of Aeronautics and Astronautics

model is larger than the rate obtained using the Gupta/CCS model for all of the trajectory conditions considered in this study. The difference in the blowing rate between the two models varies from about 15% for the 51 km case to about 25% for the 62 km conditions. The mass blowing rate is proportional to the production rate of bulk carbon. The larger rate obtained using the Wilke/Blottner/Eucken model indicates that more oxygen atoms and molecules react at the surface to form CO compared to the Gupta/CCS model. Since these oxidation reactions are exothermic, more heat is released in the form of enthalpy of formation for the Wilke/Blottner/Eucken model compared to the Gupta/CCS model, which contributes to a larger heat transfer to the surface as shown in Figure 2(a).
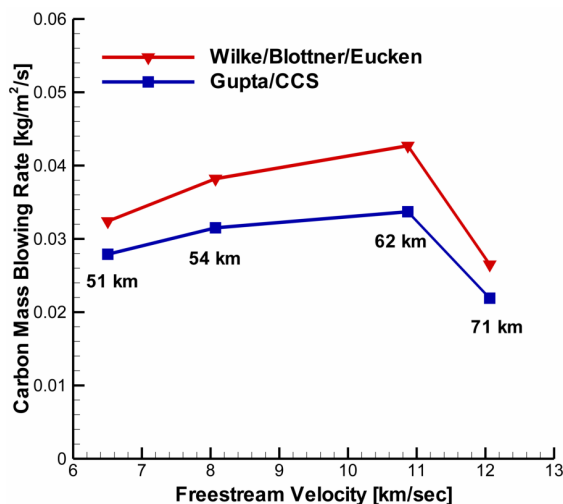
Figure 4. Mass blowing rate due to carbon oxidation calculated using the Wilke/Blottner/Eucken and Gupta/CCS models.

Figure 5 presents the mole fraction distributions of N, O, and CO through the shock layer along the stagnation line obtained using the Wilke/Blottner/Eucken and Gupta/CCS models. Figures 5(a) and 5(b) show some disagreement in the N and O distributions calculated using the two models directly downstream of the shock for the 71 km and 62 km conditions. This disagreement decreases for the 54 km and 51 km trajectory points, but there is still a difference of about 15% in the O and CO mole fractions in the shock layer calculated using the two models. The increase in the oxygen mole fraction in the boundary layer predicted using the Wilke/Blottner/Eucken model increases the production rate of CO at the surface, which increases the mass blowing rate relative to the Gupta/CCS model.

The accuracy of Wilke's mixing rule has been shown to deteriorate for temperatures above approximately 10,000 K.[4] Figure 6 shows the translational temperature distribution along the stagnation line calculated using the Wilke/Blottner/Eucken and Gupta/CCS models. The peak temperature along the stagnation line predicted using the two models is in close agreement. This peak value occurs directly downstream of the shock and varies from about 20,000 K for the 51 km trajectory point to about 60,000 K for the 71 km point. As a result, the accuracy of the Wilke/Blottner/Eucken model decreases as the altitude of the trajectory points considered in this study increases, which contributes to the differences in the heat transfer shown in Figure 3

Figure 7 presents the effective mass diffusion coefficient of N, O, and CO along the stagnation line obtained using the Wilke/Blottner/Eucken and Gupta/CCS models. Note that a single effective diffusion coefficient is defined for all of the species for the Wilke/Blottner/Eucken model (Equation 5). The results show that the effective diffusion coefficients calculated using the Gupta/CCS model are different for each species. The effective diffusion coefficient obtained using the Wilke/Blottner/Eucken model provides a reasonable approximation of the effective coefficients of N, O, and CO calculated using the Gupta/CCS model for the 54 km and 51 km conditions because the effective coefficients of these species are close. The difference between the effective diffusion coefficients calculated using the two models increases for the 71 km and 62 km conditions. For instance, the difference in the effective diffusion coefficient of N in the shock layer for the 62 km case is as large as a factor of four. The differences in the effective diffusion coefficients obtained using the two transport models also contribute to the disagreement in the heat transfer to the SRC surface.

American Institute of Aeronautics and Astronautics

(a) 71 km
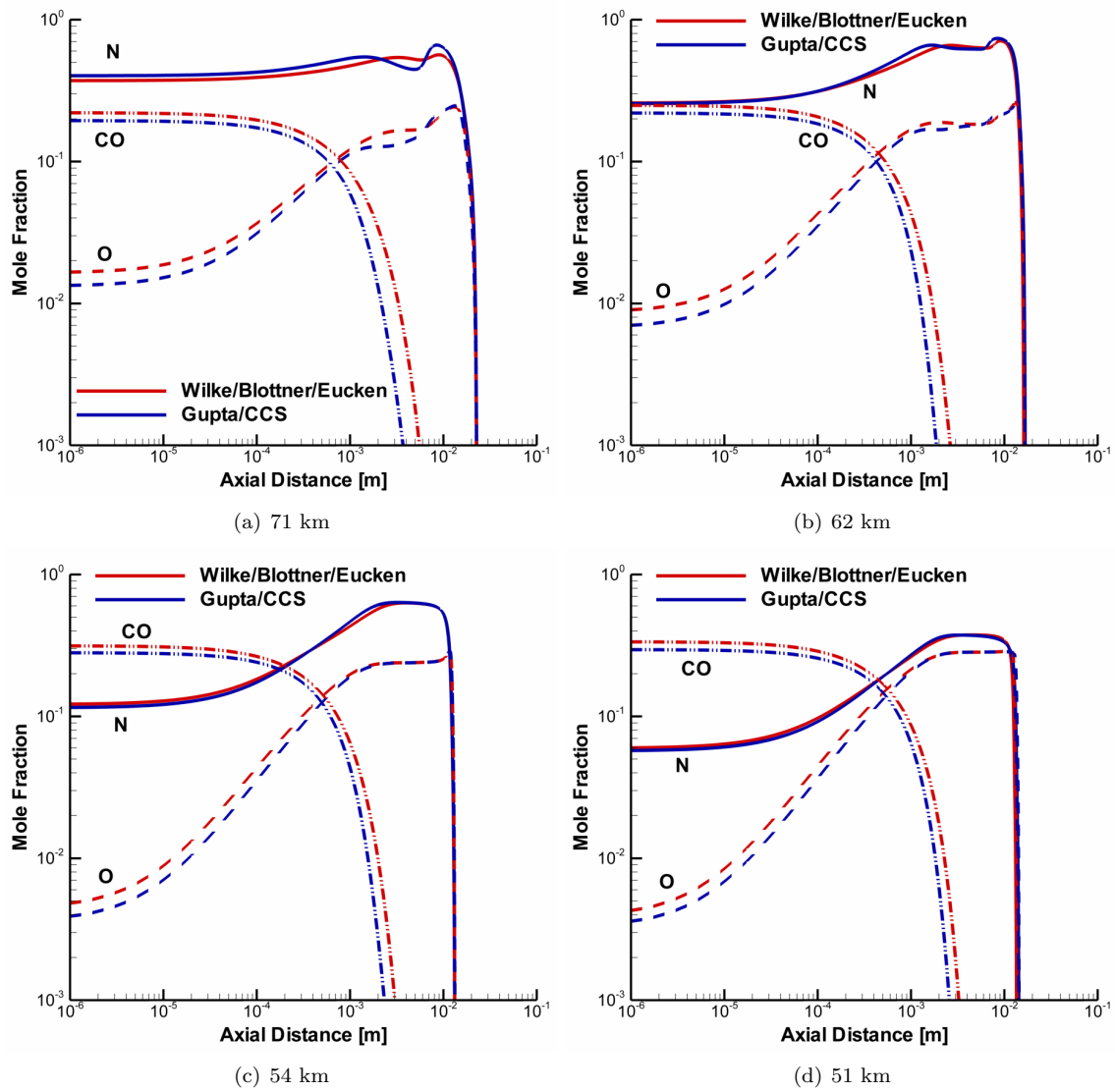
(b) 62 km

(c) 54 km

(d) 51 km

Figure 5. Mole fraction distributions of N (solid lines), O (dashed lines), and CO (dashed-dot-dot lines) along the stagnation line calculated using the Wilke/Blottner/Eucken and Gupta/CCS models.
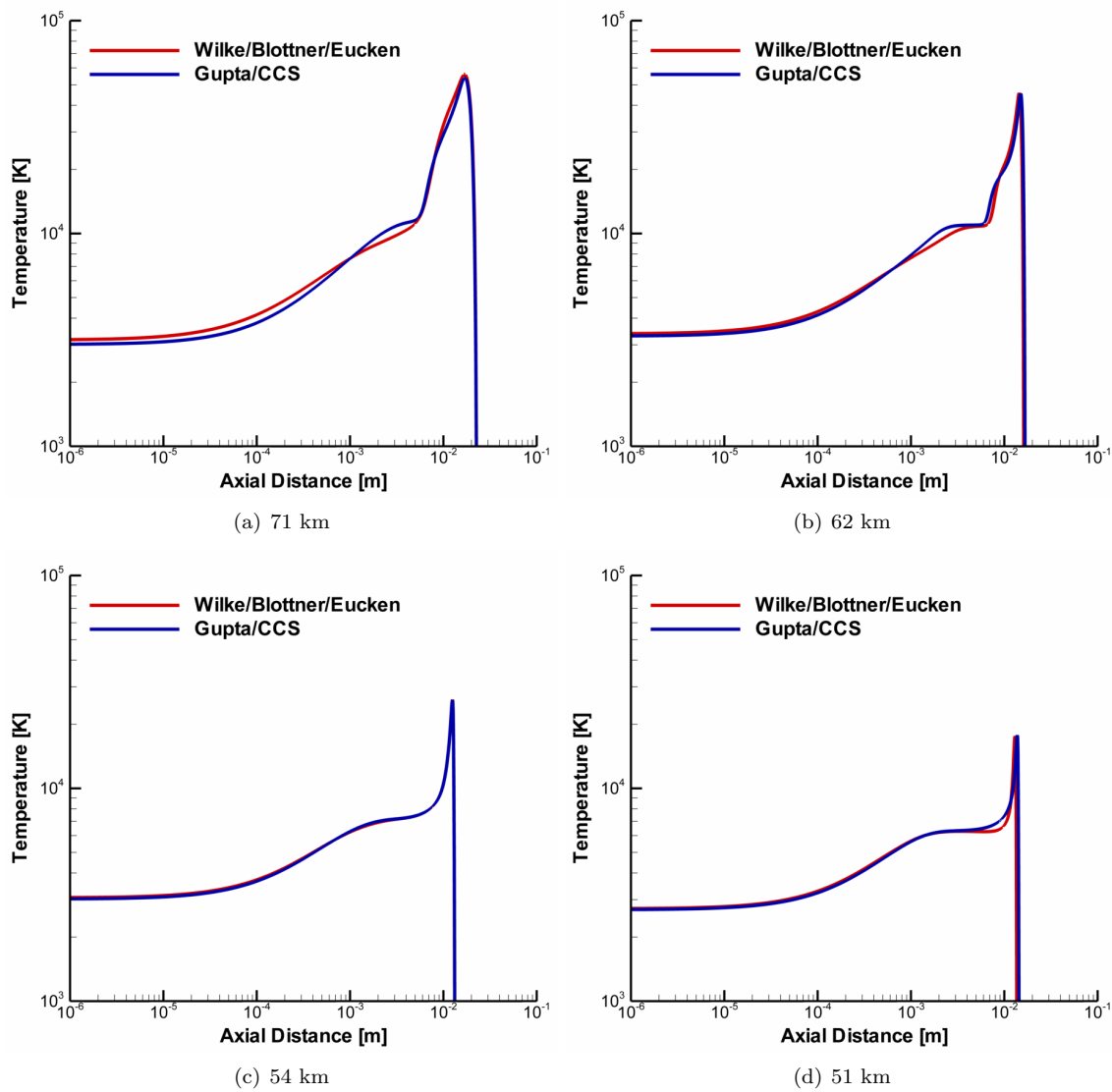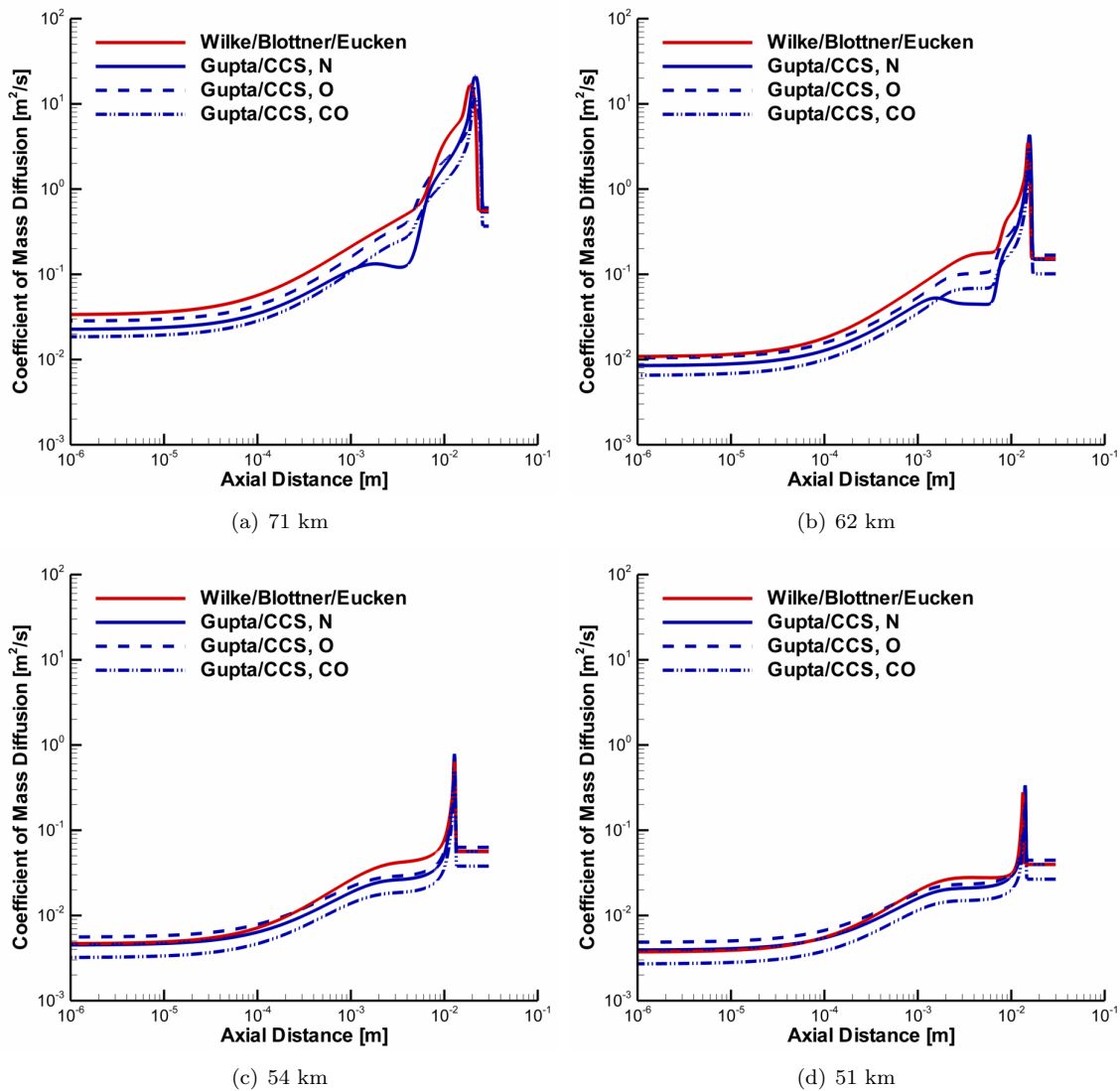
American Institute of Aeronautics and Astronautics

(a) 71 km

(b) 62 km

(c) 54 km

(d) 51 km

Figure 6.   Translational temperature distribution along the stagnation line calculated using the Wilke/Blottner/Eucken and Gupta/CCS models.

American Institute of Aeronautics and Astronautics

(a) 71 km

(b) 62 km

(c) 54 km

(d) 51 km

Figure 7. Effective diffusion coefficients of N (solid lines), O (dashed lines), and CO (dashed-dot-dot lines) along the stagnation line calculated using the Wilke/Blottner/Eucken and Gupta/CCS models.

American Institute of Aeronautics and Astronautics

B.   Mass Diffusion

In the second part of the study, the effects of the mass diffusion model on the flowfield predictions of the Stardust SRC are evaluated. Figure 8 presents the stagnation point heat transfer for the trajectory conditions considered in this study calculated using Fick's, modified Fick's, SCEBD, and Stefan-Maxwell models. The heat transfer calculated using the modified Fick's and SCEBD models are within 3% of the solution obtained using the Stefan-Maxwell model. However, Fick's model overpredicts the stagnation point heat transfer by as much as 20% for the 62 km conditions. In addition to the heat transfer calculated assuming finite-rate chemistry at the surface (Table 3), Figure 8(b) also presents the non-catalytic wall solution for comparison. Unlike the finite-rate surface chemistry solution, the heat transfer for the non-catalytic wall is not affected by the mass diffusion model for all of the entry conditions investigated in this study.
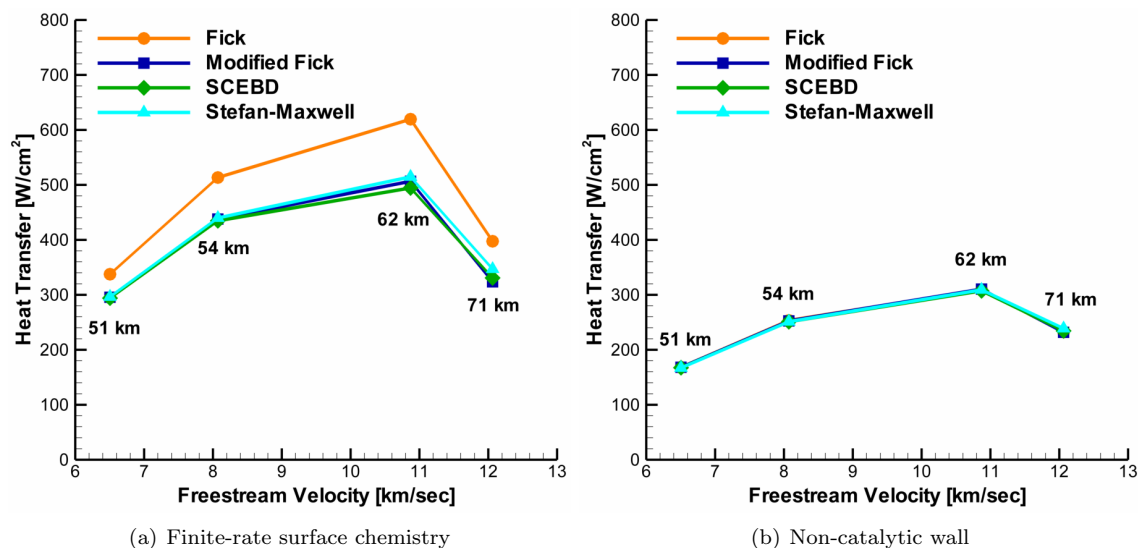

(a) Finite-rate surface chemistry (b) Non-catalytic wall

Figure 8. Stagnation point heat transfer calculated using Fick's, modified Fick's, SCEBD, and Stefan-Maxwell models.

The convective and diffusive components of the heat transfer at the stagnation point are presented in Figure 9. Figure 9(a) shows that the convective heat transfer obtained using the modified Fick's, SCEBD, and Stefan-Maxwell models are in good agreement. Fick's model produces an overall 10% larger convective heat transfer relative to the Stefan-Maxwell model. This difference in the convective heat transfer, however, is relatively small compared to the difference in the diffusive heat transfer shown in Figure 9(b). Fick's model overpredicts the diffusive heat transfer relative to the Stefan-Maxwell solution by as much as 25% (62 km). This difference in the diffusive heat transfer causes the disagreement in the stagnation point heat transfer shown in Figure 8(a).

The mass blowing rate due to the removal of bulk carbon by the oxidation mechanisms (Table 3) calculated using Fick's, modified Fick's, SCEBD, and Stefan-Maxwell models is shown in Figure 10. Similar to the heat transfer results, the mass blowing rate obtained using the modified Fick's, SCEBD, and Stefan-Maxwell models are in good agreement. Fick's model, however, predicts a larger mass blowing rate for all of the trajectory conditions considered in this study. The largest difference in the mass blowing rate between Fick's model and the Stefan-Maxwell model is approximately 20% for the 62 km conditions. This larger mass blowing rate again indicates that the heat released by the oxidation reactions is greater for Fick's model, which contributes to the larger heat transfer to the SRS surface shown in Figure 8(a).

The mole fraction distributions of N, O, and CO along the stagnation line calculated using the four mass diffusion models considered in this study are presented in Figure 11. The mole fraction in the shock layer obtained using modified Fick's, SCEBD, and Stefan-Maxwell models are in overall good agreement. The CO mole fraction near the stagnation point calculated using Fick's model is similar to the Stefan-Maxwell solution. However, the mole fractions of N and O calculated using Fick's model are larger relative to the Stefan-Maxwell solution. This disagreement in the mole fractions calculated using Fick's model compared to the Stefan-Maxwell model increases the recombination of N (to form N_2) and O (to form CO) at the surface, releasing the heats of formation and increasing the diffusive heat transfer as shown in Figure 9(b).

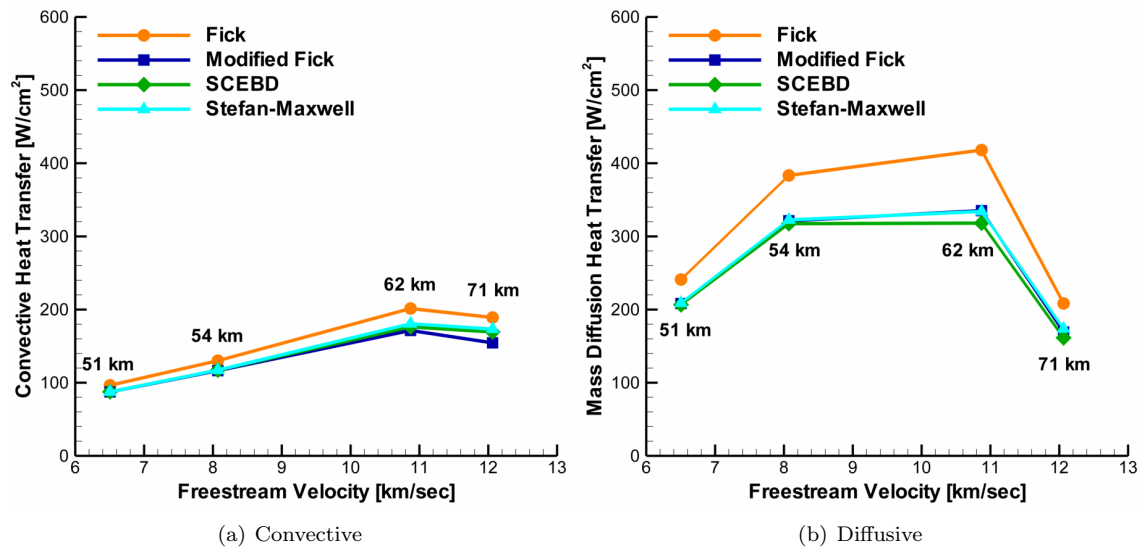American Institute of Aeronautics and Astronautics

Figure 9. Convective and diffusive stagnation point heat transfer calculated using Fick's, modified Fick's, SCEBD, and Stefan-Maxwell models.
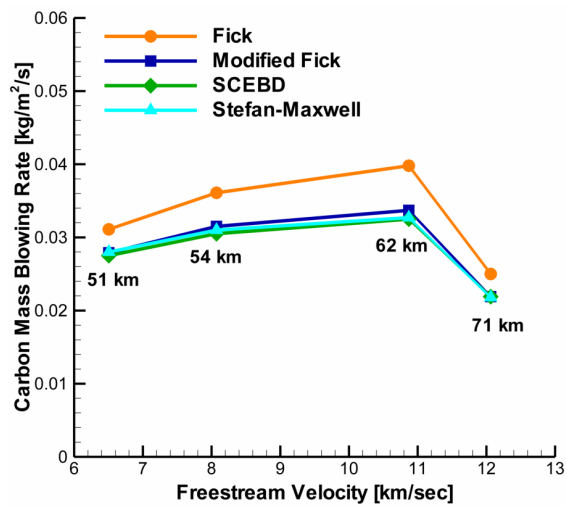

Figure 10. Mass blowing rate due to carbon oxidation calculated using Fick's, modified Fick's, SCEBD, and Stefan-Maxwell models.

American Institute of Aeronautics and Astronautics

(a) 71 km

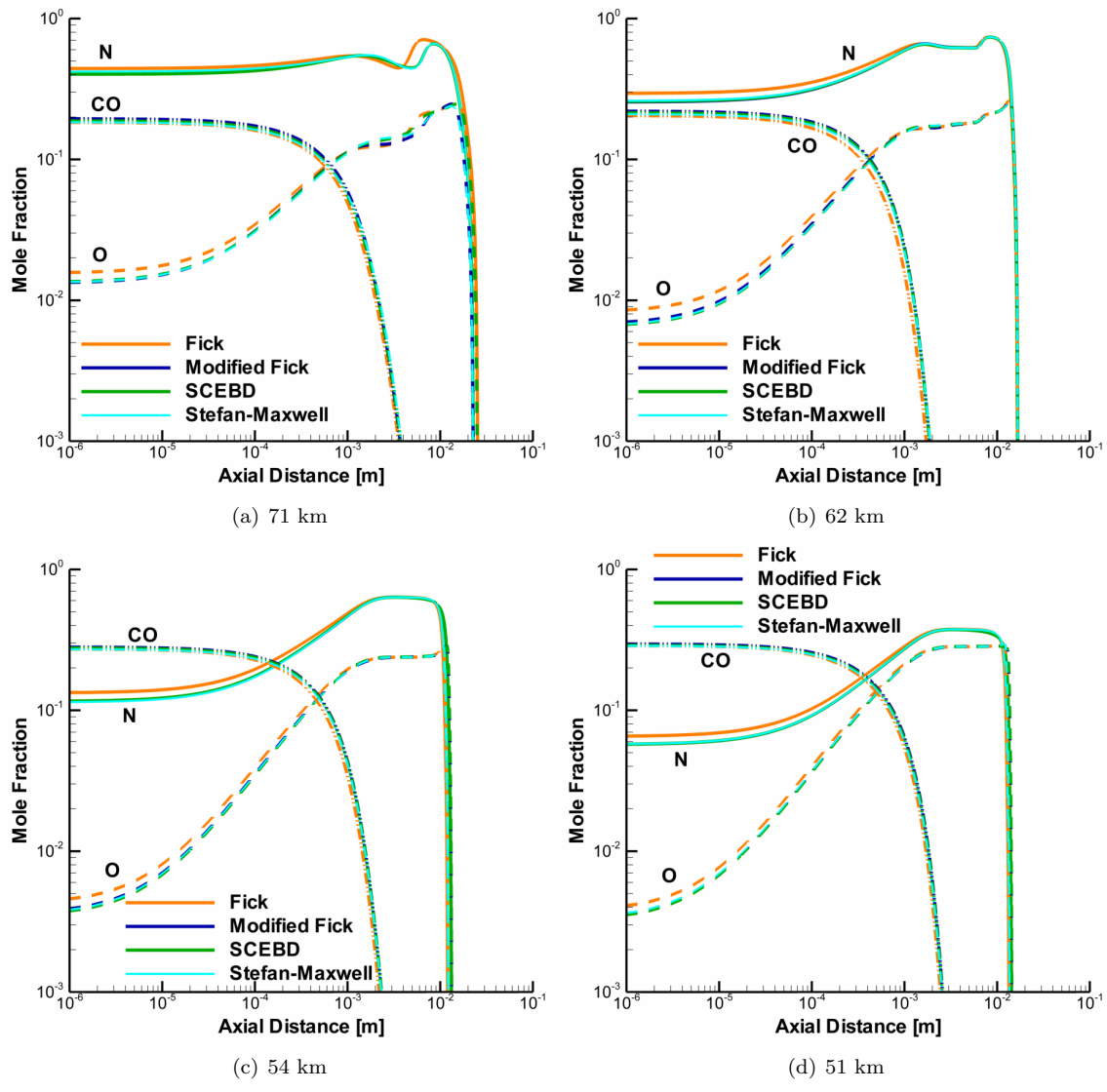(b) 62 km

(c) 54 km

(d) 51 km

Figure 11. Mole fraction distributions of N (solid lines), O (dashed lines), and CO (dashed-dot-dot lines) along the stagnation line calculated using Fick's, modified Fick's, SCEBD, and Stefan-Maxwell models.

American Institute of Aeronautics and Astronautics

V. Conclusion

The goal of this study was to evaluate the effects of the models used to calculate the transport properties of multi-component mixtures on the flowfield predictions of re-entry vehicles employing ablative heat-shields. The Stardust sample return capsule was used as the test case in this study with freestream conditions corresponding to four different trajectory points (71 km, 62 km, 54 km, and 51 km). The numerical simulations were performed using the LeMANS CFD code. Surface reactions were included using the mechanisms developed by Driver et al. for PICA and FiberForm, which include carbon oxidation and nitrogen catalysis.

In the first part of the study, the effects of the mixture transport coefficient models were assessed using two different models. The first model is Wilke's mixing rule with Blottner's curve fits and Eucken's relation used to determine the viscosity and thermal conductivities of individual species, respectively. The second model is Gupta's mixing rule with species viscosities and thermal conductivities calculated using collision cross-section data. The results showed that the heat transfer predicted using the Wilke/Blottner/Eucken model is in good agreement with the Gupta/CCS solution for relatively slow Earth entry speeds. In the context of the Stardust re-entry conditions, this corresponds to trajectory altitudes below approximately 51 km. For higher altitudes, the Wilke/Blottner/Eucken model overpredicted the heat transfer to the surface relative to the Gupta/CCS model by between approximately 15% for the 54 km conditions to 60% for the 71 km conditions. The mass blowing rate due to the removal of bulk carbon by surface reactions was also between 15% (51 km) and 25% (62 km) larger for the Wilke/Blottner/Eucken model than for the Gupta/CCS model.

The second part of the study focused on assessing the models for mass diffusion using Fick's, modified Fick's, SCEBD, and Stefan-Maxwell models. The results showed that the flowfield properties calculated using the modified Fick's, SCEBD, and Stefan-Maxwell models were in good agreement for all of the trajectory conditions considered in this study. However, Fick's model overpredicted the heat transfer and mass blowing rate for all of the trajectory conditions investigated in this study by as much as 20% (62 km) relative to the Stefan-Maxwell model. Therefore, CFD simulations of ablative heat-shields should avoid Fick's model and use either the modified Fick's model or the SCEBD model, which can efficiently replicate the flowfield solutions obtained using the Stefan-Maxwell model.

For future work, it is important to include any possible effects of the pyrolysis gases emitted from the surface. The pyrolysis gas mixture for PICA is composed of carbon and hydrogen species.[22] These species have different transport properties than air particles and the effects of the transport models can be more pronounced for these mixtures. The effects of pyrolysis gas will be assessed in future studies by coupling LeMANS with the finite-rate surface chemistry module to a material response solver. Radiative heating was neglected in this study. Future work will include any potential effects by coupling LeMANS to a radiation solver. Finally, the physical accuracy of these models will be evaluated by comparing the numerical predictions with available measurements of spectral emission data[30] made during the Stardust SRC re-entry.

Acknowledgments

References

[1]Sutton, K. and Gnoffo, P. A., "Multi-Component Diffusion with Application to Computational Aerothermodynamics," *AIAA Paper 1998-2575*, June 1998.

[2]Gosse, R. and Candler, G., "Diffusion Flux Modeling: Application to Direct Entry Problems," *AIAA Paper 2005-389*, January 2005.

[3]Chen, Y. and Milos, F. S., "Finite-Rate Ablation Boundary Conditions for a Carbon-Phenolic Heat-Shield," *AIAA Paper 2004-2270*, June 2004.

[4]Palmer, G. E. and Wright, M. J., "Comparison of Methods to Compute High-Temperature Gas Viscosity," *Journal of Thermophysics and Heat Transfer*, Vol. 17, No. 2, April-June 2003, pp. 232–239.

[5]Magin, T. E. and Degrez, G., "Transport Algorithms for Partially Ionized and Unmagnetized Plasmas," *Journal of Computational Physics*, Vol. 198, No. 2, August 2004, pp. 424449.

[6]Scalabrin, L. C., *Numerical Simulation of Weakly Ionized Hypersonic Flow over Reentry Capsules*, Ph.D. thesis, University of Michigan, 2007.

[7] Martin, A., Scalabrin, L. C., and Boyd, I. D., "High Performance Modeling of Atmospheric Re-entry Vehicles," *Journal of Physics: Conference Series*, Vol. 341, No. 1, 2012, Article 012002.

[8] MacCormack, R. W. and Candler, G. V., "The Solution of the Navier-Stokes Equations using Gauss-Seidel Line Relaxation," *Computers and Fluids*, Vol. 17, 1989, pp. 135–150.

[9] Marschall, J. and MacLean, M., "Finite-Rate Surface Chemistry Model, I: Formulation and Reaction System Examples," *AIAA Paper 2011-3783*, June 2011.

[10] MacLean, M., Marschall, J., and Driver, D. M., "Finite-Rate Surface Chemistry Model, II: Coupling to Viscous Navier-Stokes Code," *AIAA Paper 2011-3784*, June 2011.

[11] Alkandry, H., Farbar, E. D., and Boyd, I. D., "Evaluation of Finite-Rate Surface Chemistry Models for Simulation of the Stardust Reentry Capsule," *AIAA Paper 2012 [in preparation]*, June 2012.

[12] Karypis, G. and Kumar, V., "METIS: A Software Package for Partitioning Unstructured Graphs, Partitioning Meshes, and Computing Fill-Reducing Orderings of Sparse Matrices," *University of Minnesota*, 1998.

[13] Wilke, C. R., "A Viscosity Equation for Gas Mixtures," *Journal of Chemical Physics*, Vol. 18 No. 4, 1950, pp. 517–519.

[14] Blottner, F. G., Johnson, M., and Ellis, M., "Chemically Reacting Viscous Flow Program for Multi-Component Gas Mixtures," Tech. rep., SC-RR-70-754, Sandia Laboratories, Albuquerque, New Mexico, 1971.

[15] Vincenti, W. G. and Kruger, C. H., *Introduction to Physical Gas Dynamics*, Krieger Publishing Company, 2002.

[16] Gupta, R. N., Yos, J. M., Thompson, R. A., and Lee, K.-P., "A Review of Reaction Rates and Thermodynamic and Transport Properties for an 11-Species Air Model for Chemical and Thermal Nonequilibrium Calculations to 30000 K," Nasa-rp-1232, National Aeronautics and Space Administration, 1990.

[17] Wright, M. J., Bose, D., Palmer, G. E., and Levin, E., "Recommended Collision Integrals for Transport Property Computations, Part 1: Air Species," *AIAA Journal*, Vol. 43, No. 12, December 2005, pp. 2558–2564.

[18] Wright, M. J., Hwang, H. H., and Schwenke, D. W., "Recommended Collision Integrals for Transport Property Computations, Part 2: Mars and Venus Entries," *AIAA Journal*, Vol. 45, No. 1, January 2007, pp. 281–288.

[19] Kuo, K. K., *Principles of Combustion*, John Wiley & Sons, Inc., 2005.

[20] Ramshaw, J. D. and Chang, C. H., "Friction-Weighted Self-Consistent Effective Binary Diffusion Approximation," *Journal of Non-Equilibrium Thermodynamics*, Vol. 21, 1996, pp. 223–232.

[21] Ramshaw, J. D. and Chang, C. H., "Ambipolar Diffusion in Two-Temperature Multicomponent Plasmas," *Plasma Chemistry and Plasma Processing*, Vol. 13, No. 3, 1993, pp. 489–498.

[22] Tran, H. K., Johnson, C. E., Rasky, D. J., Hui, F. C. L., Hsu, M.-T., and Chen, Y. K., "Phenolic Impregnated Carbon Ablators (PICA) for Discovery class missions," *AIAA Paper 1996-1911*, June 1996.

[23] Olynick, D., Chen, Y.-K., and Tauber, M. E., "Aerothermodynamics of the Stardust Sample Return Capsule," *Journal of Spacecraft and Rockets*, Vol. 36, No. 3, May-June 1999, pp. 442–462.

[24] Martin, A., Boyd, I. D., Cozmuta, I., and Wright, M. J., "Chemistry Model for Ablating Carbon-Phenolic Material During Atmospheric Re-entry," *AIAA Paper 2010-1175*, January 2010.

[25] Martin, A. and Boyd, I. D., "CFD Implementation of a novel carbon-phenolic-in-air chemistry model for atmospheric re-entry," *AIAA Paper 2011-0143*, January 2011.

[26] Driver, D. M., Olsen, M. W., Barnhardt, M. D., and MacLean, M., "Understanding High Recession Rates of Carbon Ablators Seen in Shear Tests in an Arc Jet," *AIAA Paper 2010-1177*, January 2010.

[27] Driver, D. M. and MacLean, M., "Improved Predictions of PICA Recession in Arc Jet Shear Tests," *AIAA Paper 2011-141*, January 2011.

[28] Stackpoole, M., Sepka, S., Cozmuta, I., and Kontinos, D., "Post-flight Evaluation of Stardust Sample Return Capsule Forebody Heatshield Material," *AIAA Paper 2008-1202*, January 2008.

[29] Desai, P. N. and Qualls, G. D., "Stardust Entry Reconstruction," *Journal of Spacecraft and Rockets*, Vol. 47, No. 5, September-October 2010, pp. 736–740.

[30] Jenniskens, P., "Observations of the Stardust Sample Return Capsule Entry with a Slitless Echelle Spectrograph," *Journal of Spacecraft and Rockets*, Vol. 47, No. 5, September-October 2010, pp. 718–735.

American Institute of Aeronautics and Astronautics